*plants*

MDPI

# Uncovering Pathways Highly Correlated to NUE through a Combined Metabolomics and Transcriptomics Approach in Eggplant

Antonio Mauceri [1,*], Meriem Miyassa Aci [1], Laura Toppino [2], Sayantan Panda [3], Sagit Meir [3], Francesco Mercati [4], Fabrizio Araniti [5], Antonio Lupini [1], Maria Rosaria Panuccio [1], Giuseppe Leonardo Rotino [2], Asaph Aharoni [3], Maria Rosa Abenavoli [1,*] and Francesco Sunseri [1,4]

[1] Department Agraria, University Mediterranea of Reggio Calabria, 89122 Reggio Calabria, Italy; miyassa.aci@unirc.it (M.M.A.); antonio.lupini@unirc.it (A.L.); mpanuccio@unirc.it (M.R.P.); francesco.sunseri@unirc.it (F.S.)

[2] CREA—Research Centre for Genomics and Bioinformatics, 26836 Montanaso Lombardo, Italy; laura.toppino@crea.gov.it (L.T.); giuseppeleonardo.rotino@crea.gov.it (G.L.R.)

[3] Department of Plant and Environmental Sciences, Weizmann Institute of Science, Rehovot 7610001, Israel; sayantan.panda@weizmann.ac.il (S.P.); sagit.meir@weizmann.ac.il (S.M.); asaph.aharoni@weizmann.ac.il (A.A.)

[4] Institute Bioscience and Bioresources—National Research Council CNR, 90129 Palermo, Italy; francesco.mercati@ibbr.cnr.it

[5] Department of Agricultural and Environmental Sciences—Production, Territory, Agroenergy, University of Milano, 20133 Milan, Italy; fabrizio.araniti@unimi.it

* Correspondence: antonio.mauceri87@unirc.it (A.M.); mrabenavoli@unirc.it (M.R.A.)

**Abstract:** Nitrogen (N) fertilization is one of the main inputs to increase crop yield and food production. However, crops utilize only 30–40% of N applied; the remainder is leached into the soil, causing environmental and health damage. In this scenario, the improvement of nitrogen-use efficiency (NUE) will be an essential strategy for sustainable agriculture. Here, we compared two pairs of NUE-contrasting eggplant (*Solanum melongena* L.) genotypes, employing GC-MS and UPLC-qTOF-MS-based technologies to determine the differential profiles of primary and secondary metabolites in root and shoot tissues, under N starvation as well as at short- and long-term N-limiting resupply. Firstly, differences in the primary metabolism pathways of shoots related to alanine, aspartate and glutamate; starch, sucrose and glycine; serine and threonine; and in secondary metabolites biosynthesis were detected. An integrated analysis between differentially accumulated metabolites and expressed transcripts highlighted a key role of glycine accumulation and the related *glyA* transcript in the N-use-efficient genotypes to cope with N-limiting stress. Interestingly, a correlation between both sucrose synthase (*SUS*)- and fructokinase (*scrK*)-transcript abundances, as well as D-glucose and D-fructose accumulation, appeared useful to distinguish the N-use-efficient genotypes. Furthermore, increased levels of L-aspartate and L-asparagine in the N-use-efficient genotypes at short-term low-N exposure were detected. Granule-bound starch synthase (*WAXY*) and endoglucanase (*E3.2.1.4*) downregulation at long-term N stress was observed. Therefore, genes and metabolites related to these pathways could be exploited to improve NUE in eggplant.

**Keywords:** *Solanum melongena* L.; primary metabolites; GC-MS; glycoalkaloids; UPLC-qTOF-MS; RNA-seq; nitrogen-use efficiency

## 1. Introduction

Soil-N availability is one of the most important factors limiting worldwide plant growth and productivity. Nitrogen limitation leads to many functional damages, inducing alterations in physiological, biochemical, and molecular processes such as photosynthesis, respiration, ion uptake and translocation, carbon metabolism, and senescence [1,2]. Over

the last four decades, N employed in fertilization has dramatically increased in order to maximize crop yield and consequently meet food demands [3]. However, excessive use of N determines negative effects on the environment, economy, and human health [4]. Thus, nitrogen-use-efficiency (NUE) improvement in crop plants, together with low-N-fertilizer input and best-management practices, could represent strategies to limit the negative impact of agriculture on the environment and human health [5].

NUE, defined as "the grain yield per unit of N available in the soil", is a complex trait under physiological, biochemical, and genetic control [6,7]. Efforts have been made to identify molecular mechanisms underlying NUE to improve this complex trait by conventional breeding programs in several crops [8]. Recently, metabolomics, transcriptomics, and proteomics are becoming valuable tools in model and crop species to understand changes in biological processes, genes, and chemical composition of primary and secondary metabolites involved in stress responses, including N deficiency [9–11].

NUE has been mainly explored in several crop plants, such as rice, wheat, and maize [12], but should be relevant also for *Solanaceae* crops due to their high dependence in N fertilizers [13]. Limited information on NUE is available on eggplant (*Solanum melongena* L.), the third most important vegetable crop (following tomato and potato) that is cultivated worldwide, mainly in Asian territories [13]. Recently, two NUE-contrasting genotypes have been identified in hydroponic and greenhouse experiments, under low-N conditions [14]. Transcriptome analysis, in both shoot and root tissues, highlighted differentially expressed genes (DEGs) related to NUE traits after short- and long-term N-stress exposure. In detail, DEGs involved in the light-reaction pathway, the response to inorganic substances, abiotic stimulus, and cellular response to N starvation, together with several putative transcription factors (TFs) were upregulated in the N-use-efficient genotypes [15].

Here, we use a metabolomics approach to examine the metabolic profiles of NUE-contrasting genotypes [14], with particular emphasis to organic acids, amino acids, sugars, and secondary metabolites, mainly on nitrogen-containing ones such as glycoalkaloids that previously have been considered. In particular, glycoalkaloids (GAs), a class of nitrogen-containing secondary metabolites, commonly occur in the *Solanaceae* family (tomato, potato, and eggplant). Although considered toxic for human health, they exhibit a wide range of pharmacological properties, including anticancer activity; whereas in plants, they play an important defense role against pests [16,17]. Interestingly, plants change their metabolic profiles under N stress, according to the starvation period, genotypes, and tissues [18,19]. In particular, N- and C-containing metabolites (including organic acids) are strictly correlated with plant biomass and growth [20].

To identify key pathways involved in N metabolism in eggplant, an integration between metabolomics and transcriptomics data was carried out. Our findings shed light on genes and metabolites reprogrammed in N-use-efficient genotypes compared to inefficient genotypes under N-limiting resupply, providing valuable knowledge to develop strategies for improving NUE in eggplant.

## 2. Results

### 2.1. Metabolite Detection in Contrasting NUE Genotypes at Different Resupply Time Intervals

Root and shoot extracts derived from high (AM222 and 67-3)- and low (305E40 and AM22)-NUE eggplant genotypes were profiled using GC-MS (mainly primary, polar metabolites) and high-resolution MS (HRMS; UPLC-qTOF-MS; mainly secondary, semi-polar metabolites) to examine the plant response to N starvation as well as short- and long-term N-limited resupply. In both tissues, collected at $T_0$ (after 2 days N-free solution), $T_1$ and $T_2$ (1 and 16 days after $NO_3^-$ resupply), 33 (through GC-MS) and 29 (through UPLC-qTOF-MS) metabolites were annotated in high confidence. GC-MS analysis results in the identification of three main primary metabolite classes including amino acids (17), organic acids (11), and sugars (5) (Supplementary Table S1A). In HRMS analysis, we focused on nitrogen-containing metabolites, mainly glycoalkaloids (Supplementary Table S1B).

## 2.2. Multivariate Statistical Analysis of Eggplant Metabolite

The PCA model performed on root data took into account the two main components, PC1 vs. PC2, which explained 31.6% and 9.4% of the total variance (41%), respectively. The analysis did not clearly separate the samples (Figure 1A). Loading plots of metabolites according to different times and genotypes in root are shown in Supplementary Table S2A. Conversely, in shoot, PC1 and PC2 explained 20.4% and 15% of the total variance (35.4%), respectively, pointing out proximity between time sampling $T_0$ and $T_1$, while $T_2$ appeared more distinguished (Figure 1B). The more N-use-efficient genotypes, AM222, 305E40, and 67-3, showed distinct metabolic profiles (in $T_2$); by contrast, the AM22 did not show any significant difference across the time of sampling (Figure 1B, Supplementary Table S2B).
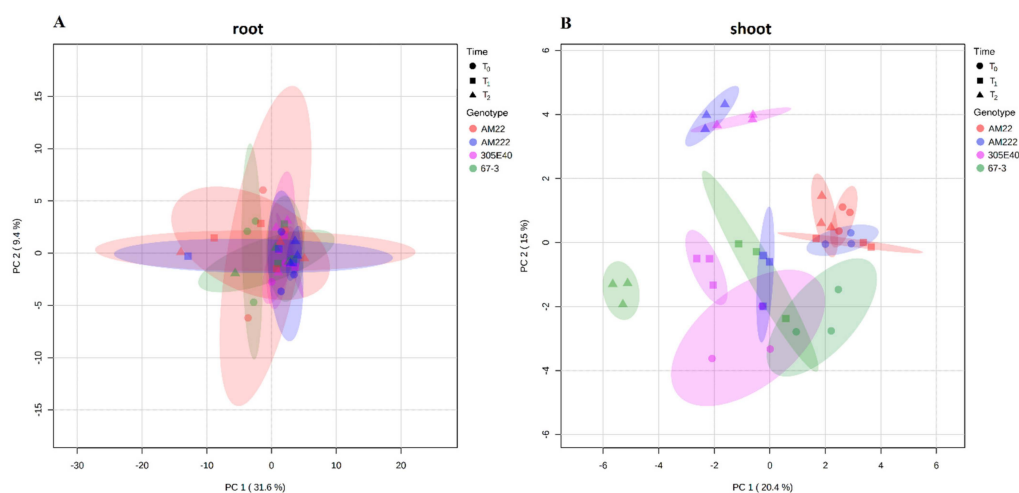


**Figure 1.** Two-dimensional plot of principal component analysis (PCA) of eggplant metabolites for root (**A**) and shoot (**B**). The dots represent accessions with 95% confidence regions as ellipses. (**A**) In root, PC1 and PC2 explained 41% of total variation; time sampling and accessions are not clearly distinguished. (**B**) In shoot, PC1 and PC2 explained 35.4% of total variations; AM22 do not respond to N limitation, while the other genotypes are clearly distinguished by treatments (time).

To maximize the variance, a partial least-squares discriminant analysis (PLS-DA) was performed on the same datasets. In root, the PLS-DA permutation test showed an empirical *p*-value $\geq 0.05$; therefore it was not considered. In shoot, the PLS-DA model defined a clearer separation, on which components 1 and 2 explained 13.9% and 12.1% of the total variance, respectively. At all sampling times, the replicates of each genotype were closely grouped (apart from the AM222 samples at $T_1$; Figure 2). AM22 displayed reduced metabolic changes across sampling times ($T_0$, $T_1$, and $T_2$) compared to the other genotypes. Notably, at $T_2$, the high-NUE genotypes (i.e., AM222 and 67-3), appeared well-separated from 305E40 and AM22 (the lower-NUE genotypes; Figure 2A). The variable importance in projection (VIP) indicated L-glutamine, L-isoleucine, L-cysteine, myo-inositol, L-phenylalanine, solamargine isomer (M869T830), shikimic, L-glutamic, oxalic, and succinic acids as the most discriminant metabolites among the genotype-profile scores (Figure 2B, Supplementary Table S3B). More specifically, at $T_0$, the low-NUE genotype AM22 showed high levels of L-glutamic acid, L-cysteine, and L-isoleucine, while 305E40 showed high levels of L-glutamine. Conversely, in the high-NUE genotypes, 67-3 exhibited high levels of the unknown glycoalkaloid M1003T1070, while AM222 the solamargine isomer (M869T830). At $T_1$, AM22, and 305E40 accumulated shikimic acid and L-phenylalanine, respectively. Furthermore, 67-3 and AM222 showed high levels of oxalic acid and the solamargine isomer (M869T830), as well as L-cysteine. Finally, at $T_2$, AM22 accumulated succinic acid, L-glutamic acid, and myo-inositol, while 305E40 exhibited high levels of solamargine isomer (M869T830), L-isoleucine, and L-leucine (Figure 2B, Supplementary Table S3B).
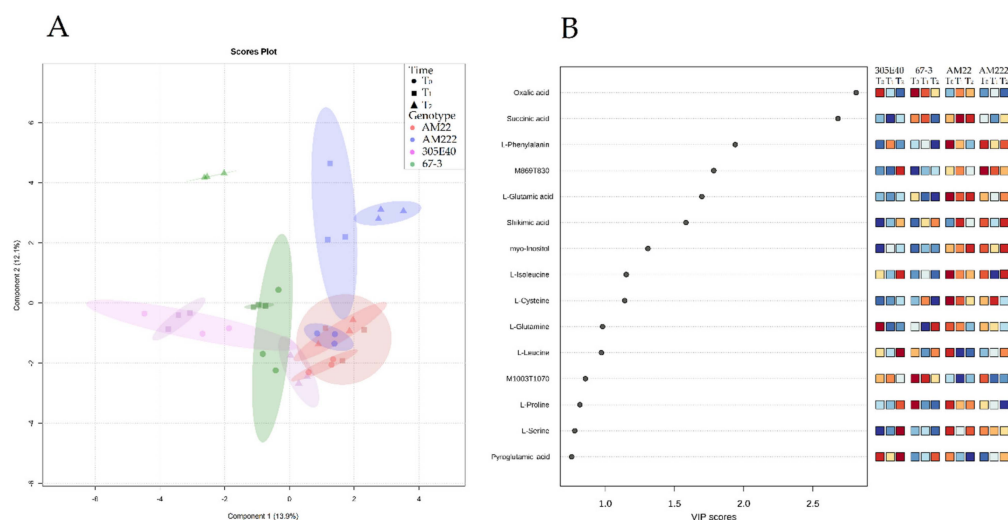
**Figure 2.** Partial least-squares discriminant analysis (PLS-DA) in shoot. (**A**) 2D scores plot of PLS-DA; the dots represent accessions with 95% confidence regions as ellipses. (**B**) The importance measures used in PLS-DA are VIP scores (variable importance in projection). The colored boxes on the right indicate the relative concentrations of the corresponding metabolite in each group.

### 2.3. Root and Shoot Metabolites in Eggplant Genotypes under Low N Supply

The analysis of variance (ANOVA), comparing the overall variation among the identified metabolites ($p < 0.05$), is provided in Supplementary Table S4A,B. In the root tissue, differences were mainly observed in secondary metabolites while only the myo-inositol was changed among the primary ones. In particular, at $T_0$, the N-use-inefficient genotype AM22 showed significant accumulation of secondary metabolites, mainly furostanol and the soladulcine A, together with myo-inositol (Figure 3A), while at $T_1$ and $T_2$, the secondary metabolites were gradually reduced. Interestingly, at $T_1$, the efficient genotype AM222 displayed an increase in solasonine (S) (M885T1016), solamargine isomer (M869T830), solasonine isomer (M885T1031), and hydroxy dihydro solasonine (M903T687) (Figure 3B). In contrast to root, the shoot tissue showed differences in both primary and secondary metabolites (Figure 4). D-glucose and D-fructose showed the highest levels among sugars, while L-aspartic and L-glutamic acids, L-isoleucine, L-proline, L-glutamine, L-phenylalanine, L-asparagine, L-threonine, L-cysteine, and glycine showed highest levels among the amino acids. Finally, L-malic, oxalic, succinic, shikimic, glyceric, and fumaric acids appeared significantly variable among the organic acids comparing sampling times and genotypes (Figure 4). The glycoalkaloids solamargine isomer (M869T830), hydroxy dihydro solamargine (M887T705), hydroxy-solamargine isomer 1 (M885T703), unsaturated unidentified glycoalkaloid (UGA; M862T924), and unsaturated malonyl furostanol type saponin (M1118T1173) were differentially accumulated (Figure 4).

More specifically, the N-use-efficient genotype AM222 showed the highest levels of L-malic and shikimic acids as well as D-glucose at N starvation ($T_0$); conversely the N-use-inefficient AM22 exhibited the highest levels of fumaric and glyceric acids, several amino acids, and secondary metabolites (Figure 4A). At $T_1$, AM222 showed the highest level of L-serine, L-valine, and L-leucine, while AM22 showed the highest levels of D-glucose and D-fructose as well as fumaric and shikimic acids (Figure 4B). Finally, at $T_2$, AM222 exhibited the highest level of shikimic acid and D-glucose as well as secondary metabolites, while oxalic, succinic, L-aspartic, and L-glutamic acids accumulated more in AM22 than AM222 (Figure 4C).
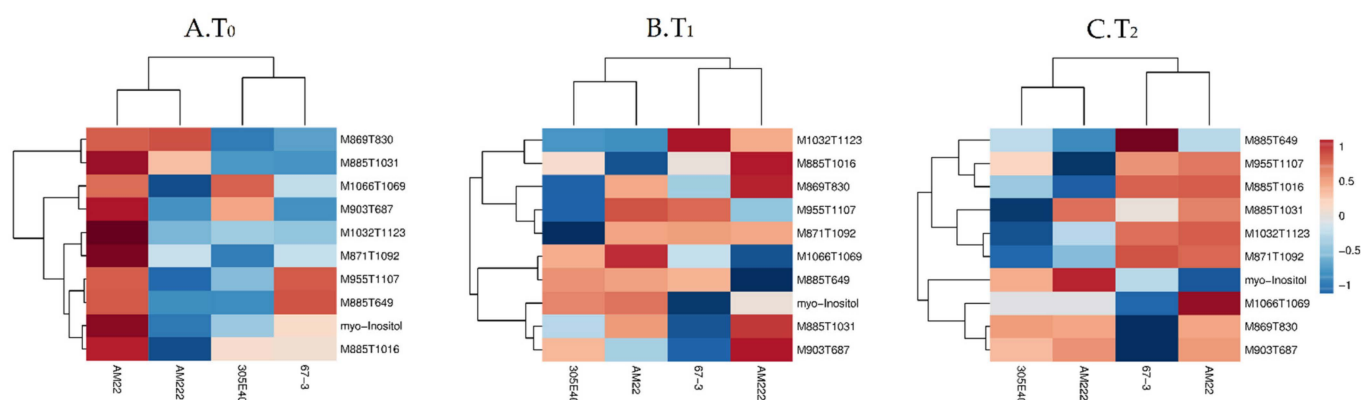
**Figure 3.** Heatmap of metabolites significantly differentially abundant among genotypes in root (one-way ANOVA and post hoc with $p \leq 0.05$). Each column and row represent a sample and a metabolite, respectively. Comparison among genotypes shows that the main differences are in the secondary metabolites at $T_0$ (**A**), $T_1$ (**B**), and $T_2$ (**C**).
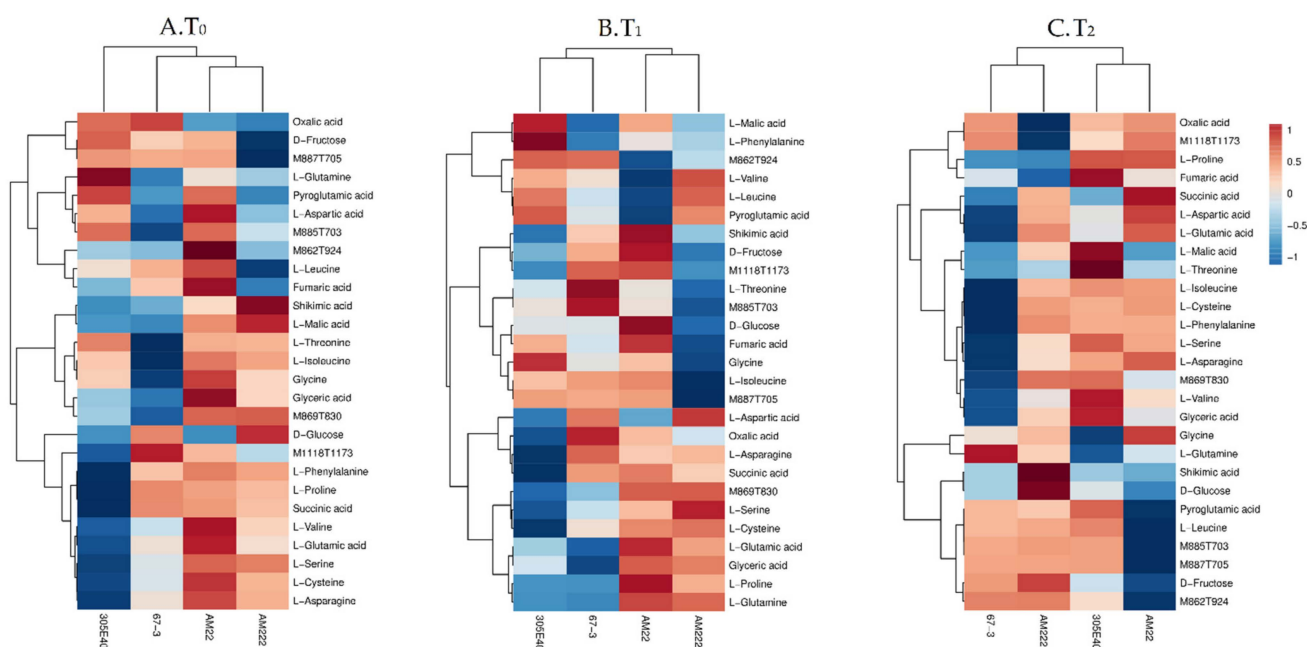


**Figure 4.** Heatmap of metabolites significantly differentially abundant among genotypes in shoot (one-way ANOVA and post hoc with $p \leq 0.05$). Each column and row represent a sample and a metabolite, respectively. Comparison among genotypes shows that the main differences are in the primary metabolites at $T_0$ (**A**), $T_1$ (**B**), and $T_2$ (**C**).

## 2.4. Comparative Changes in the Primary Metabolite Pathways in Shoot

Significant different metabolic pathways ($p < 0.05$, FDR < 0.05, and impact >0.2) were identified by pairwise comparisons among genotypes at the same sampling time, among which are alanine, aspartate and glutamate (impact 0.65); glycine, serine and threonine (impact 0.54); phenylalanine (impact 0.47); starch and sucrose (impact 0.39); and glyoxylate and dicarboxylate (impact 0.28) (Table 1).

**Table 1.** Comparative changes in the primary metabolite pathways in shoot. Metabolic pathways with FDR < 0.05 and higher impact values are highlighted. Pairwise comparison between genotypes. Total Cmpd represents the total compound number in the pathway; Hits is the actual matched number from the uploaded data; Raw p is the original *p* value calculated from the enrichment analysis; Holm p is the *p* value adjusted by Holm–Bonferroni method; FDR p is the *p* value adjusted using false discovery rate; Impact is the pathway impact value calculated from pathway topology analysis.

| Pairwise Comparison in Shoot | Pathway Analysis | Total Cmpd | Hits | Raw p | −log(p) | Holm Adjust | FDR | Impact |
|---|---|---|---|---|---|---|---|---|
| $T_0$_67-3_*vs*_AM22 | Alanine, aspartate, and glutamate metabolism | 22 | 7 | 0.020155 | 1.6956 | 0.50388 | 0.047029 | 0.64748 |
| $T_0$_305E40_*vs*_AM22 | | | | 0.002014 | 2.6959 | 0.068486 | 0.0094 | |
| $T_1$_AM222_*vs*_AM22 | | | | 0.00278 | 2.5559 | 0.088969 | 0.010616 | |
| $T_1$_67-3_*vs*_AM22 | | | | $1.99 \times 10^{-5}$ | 4.7012 | 0.00077607 | 0.000209 | |
| $T_1$_305E40_*vs*_AM22 | | | | $2.3 \times 10^{-5}$ | 4.6388 | 0.00094188 | 0.00029 | |
| $T_2$_AM222_*vs*_AM22 | Starch and sucrose metabolism | 22 | 2 | 0.003484 | 2.458 | 0.13935 | 0.038299 | 0.39104 |
| $T_2$_67-3_*vs*_AM22 | Alanine, aspartate, and glutamate metabolism | 22 | 7 | 0.000618 | 3.2088 | 0.021642 | 0.003246 | 0.64748 |
| $T_2$_305E40_*vs*_AM22 | Glycine, serine, and threonine metabolism | 33 | 5 | 0.000335 | 3.4751 | 0.013731 | 0.00559 | 0.53598 |
| $T_0$_305E40_*vs*_AM222 | Aminoacyl-tRNA biosynthesis | 46 | 14 | 0.00032 | 3.4948 | 0.013443 | 0.013443 | 0.11111 |
| $T_1$_305E40_*vs*_AM222 | Alanine, aspartate, and glutamate metabolism | 22 | 7 | $4.37 \times 10^{-5}$ | 4.3594 | 0.0016609 | 0.000367 | 0.64748 |
| $T_2$_305E40_*vs*_AM222 | | | | 0.007058 | 2.1513 | 0.26116 | 0.049408 | |
| $T_1$_67-3_*vs*_AM222 | Alanine, aspartate, and glutamate metabolism | 22 | 7 | 0.001201 | 2.9203 | 0.043252 | 0.007209 | 0.64748 |
| $T_2$_67-3_*vs*_AM222 | Phenylalanine metabolism | 11 | 1 | $9.78 \times 10^{-5}$ | 4.0098 | 0.0040085 | 0.000851 | 0.47059 |
| $T_0$_67-3_*vs*_305E40 | Glyoxylate and dicarboxylate metabolism | 29 | 9 | 0.002673 | 2.5731 | 0.10691 | 0.037417 | 0.28209 |
| $T_1$_67-3_*vs*_305E40 | Alanine, aspartate, and glutamate metabolism | 22 | 7 | $2.06 \times 10^{-5}$ | 4.6871 | 0.00078109 | 0.000173 | 0.64748 |
| $T_2$_67-3_*vs*_305E40 | | | | 0.001274 | 2.8949 | 0.033116 | 0.003147 | |

To identify differently accumulated metabolites in each pathway, a comparison between AM22, the most N-use-inefficient, and all other genotypes was performed (Supplementary Figure S1; all the other comparisons are given in Supplementary Table S5). At $T_0$, 67-3 showed a significant reduction in L-aspartate, while 305E40 exhibited a significant lower L-glutamate and succinate content compared to AM22 (Supplementary Figure S1A,B). At $T_1$, AM222 and 67-3 showed a higher content in L-aspartate and a lower level in L-glutamate; by contrast, 305E40 evidenced a decrease in L-glutamine, L-glutamate, and succinate content compared to AM22 (Supplementary Figure S1C–E). At $T_2$, AM222 significantly differed in starch and sucrose metabolism compared to AM22, with a higher content in sucrose and D-glucose (Supplementary Figure S1G). By contrast, 67-3 showed a reduction in L-asparagine, L-alanine, L-glutamate, and succinate content (Supplementary Figure S1G). Finally, 305E40 displayed an increase in D-glycerate and L-threonine content, as well as a decrease in glycine as compared to AM22 (Supplementary Figure S1H).

### 2.5. Metabolite- and Transcript-Correlation Analysis

To investigate the pathways most significantly affected by N-limiting condition in the NUE-contrasting eggplants, we performed an integrated analysis of metabolomics and transcriptomics datasets [15] obtained by the same experimental setup. KEGG database was used to annotate the eggplant genes in the same pathway. Thus, 121 genes including 17, 13, 33, 21, 7, 26, and 4 genes, respectively, from the aminoacyl-tRNA biosynthesis (ko00970); the alanine, aspartate, and glutamate metabolism (ko00250); the starch and sucrose metabolism (ko00500); the glycine, serine, and threonine metabolism (ko00260); the phenylalanine metabolism (ko00360); the glyoxylate and dicarboxylate metabolism (ko00630); and the isoquinoline alkaloid biosynthesis (ko00950, related to the secondary metabolism), were identified (Supplementary Table S6).

To build a correlation network between metabolites and gene transcripts, a Pearson's correlation on a 121-genes and 39-metabolite dataset from both tissues was performed. Seventy (70) correlated variables (Supplementary Table S7) were highlighted with a correlation coefficient $\geq 0.70$ and $\leq -0.70$ and a *p*-value $< 0.05$ (Supplementary Figure S2A,B). These 70 correlated variables were then subjected to pathway-enrichment analysis, which identified the most significant metabolic pathway (impact $\geq 0.6$) affected by treatments in the glycine, serine, and threonine; starch and sucrose; and glyoxylate and dicarboxylate metabolism pathways (Supplementary Figure S2C). Metabolite and gene differences and their correlations were visualized through a heatmap for each genotype and time sampling ($T_0$, $T_1$ and $T_2$). The N-use-efficient (AM222 and 67-3) and inefficient (305E40 and AM22) genotypes clustered separately in shoot at $T_0$ and $T_1$, while a clustering between NUE-contrasting genotypes was also observed in root at $T_1$. At $T_2$, in both tissues, AM222 and AM22, the more contrasting genotypes for NUE clustered distinctly (Supplementary Figures S3–S5, Table S8).

### 2.6. Genotype Clustering and Responses to Nitrogen Starvation

At $T_0$, in shoot the N-use-efficient genotypes, AM222 and 67-3, clustered due to differences in transcript abundances of sucrose synthase (*SUS*; SMEL_007g277290.1), a component of starch and sucrose metabolism; glycine hydroxy methyltransferase (*glyA*; SMEL_005g228290.1; synonym of *shmt1*, serine hydroxymethyltransferase 1) and dihydrolipoamide dehydrogenase (*DLD*; SMEL_005g227630.1) components of glycine, serine, and threonine metabolism; and malate dehydrogenase (*MDH1*; SMEL_009g332450.1) and isocitrate lyase (*aceA*; SMEL_007g288630.1) which are involved in glyoxylate and dicarboxylate metabolism. A higher accumulation in D-fructose in AM222 was also observed (Supplementary Figure S3A). By contrast, AM22 and 305E40, the N-use-inefficient genotypes, accumulated more transcripts of the polyphenol oxidase (*PPO*; SMEL_000g064350.1, isoquinoline alkaloid biosynthesis), two different sucrose synthase isoforms (*SUS*; SMEL_007g277310.1 and SMEL_012g382160.1), and 4-alpha-glucanotransferase (*malQ*; SMEL_007g279110.1). They further showed an upregulation in the phenylalanine decarboxylase (*AADC*;

SMEL_008g301360.1) and phenylalanine ammonia-lyase (*PAL*; SMEL_005g230690.1) involved into phenylalanine metabolism. AM22 and 305E40 showed also a higher accumulation of fumaric acid as well as all the glycoalkaloids (Supplementary Figure S3A).

At $T_0$, in root, the glyoxylate/succinic semialdehyde reductase (*GLYR*; SMEL_000g004100.1), granule-bound starch synthase (*WAXY*; SMEL_000g036450.1) and glutamate decarboxylase (*GAD*; SMEL_001g150880.1) appeared upregulated in AM22 together with a higher accumulation in myo-inositol compared to the other genotypes; by contrast in 305E40, the amidophosphoribosyltransferase (*purF*; SMEL_001g116660.1), threonine synthase (*thrC*; SMEL_003g 197730.1), glucan endo-1,3-beta-glucosidase 4 (*GN4*; SMEL_001g152910.1) and isocitrate lyase (*aceA*; SMEL_007g288630.1) were upregulated compared to the others, accompanied by a higher accumulation of secondary metabolites. Furthermore, a strong downregulation of starch synthase (*glgA*; SMEL_000g085440.1) and a lower accumulation of L-alanine was exhibited (Supplementary Figure S3B).

## 2.7. Genotype Clustering and Short-Term Responses to Low Nitrogen Supply

At $T_1$, in shoot, two distinguishable clusters between the N-use-efficient genotypes and the inefficient ones were generated (Supplementary Figure S4). The AM222 and 67-3 showed an upregulation of the granule-bound starch synthase (*WAXY*; SMEL_000g036450.1) and endoglucanase (*E3.2.1.4*; SMEL_003g177010.1) involved in the starch and sucrose metabolism, as well as phenylalanine decarboxylase (*AADC*; SMEL_005g228290.1) and glycine hydroxy methyltransferase (*glyA*; SMEL_000g004730.1) comprised in the glyoxylate and dicarboxylate metabolism (Supplementary Figure S4A).

Otherwise, the AM22 and 305E40 evidenced an upregulation of many genes involved in different pathways (Supplementary Figure S4A). In particular, the glycine dehydrogenase (*GLDC*; SMEL_008g307820.1; glyoxylate and dicarboxylate metabolism) transcripts appeared more expressed together with a higher accumulation in D-glucose and sucrose; the isocitrate lyase (*aceA*; SMEL_007g288630.1; glyoxylate and dicarboxylate metabolism) was upregulated together with myo-inositol; the alanyl-tRNA and aspartyl-tRNA synthetases (*AARS*; SMEL_001g115360.1 and *DARS2*; SMEL_000g033540.1 in the aminoacyl-tRNA biosynthesis) were upregulated, accompanied by a higher accumulation in fumaric acid and L-alanine. Interestingly, these genotypes confirmed a higher accumulation of all the glycoalkaloids compared to the N-use-efficient genotypes as already observed at $T_0$ (Supplementary Figure S4A).

At $T_1$, two distinct clusters between the NUE-contrasting genotypes were confirmed in root. The efficient genotypes showed a significant upregulation of the endoglucanase (*E3.2.1.4*; SMEL_003g177010.1) and sucrose synthase isoform (*SUS*; SMEL_003g277290.1) involved in the starch and sucrose metabolism (Supplementary Figure S4B). By contrast, the (S)-2-hydroxy-acid oxidase (*HAO*; SMEL_004g202790.1; glyoxylate and dicarboxylate metabolism) resulted down-regulated. In the N-use-inefficient genotype 305E40, another sucrose synthase isoform (*SUS*; SMEL_012g382160.1), and trehalose 6-phosphate synthase/phosphatase (*TPS*; SMEL_001g151160.1), involved into the starch and sucrose metabolism, were upregulated concurrently with a higher accumulation of several secondary metabolites (Supplementary Figure S4B). It also exhibited a higher glucan endo-1,3-beta-glucosidase 4 (*GN4*; SMEL_001g152910.1) and 4-alpha-glucano transferase (*malQ*; SMEL_007g279110.1) transcripts abundances in the starch and sucrose metabolism as well as the aspartate-semialdehyde dehydrogenase (*asd*; SMEL_001g151200.1; glycine, serine, and threonine metabolism) and amidophosphoribosyl-transferase (*purF*; SMEL_001g116660.1; alanine, aspartate, and glutamate metabolism) (Supplementary Figure S4B).

## 2.8. Genotype Clustering and Long-Term Responses to Low Nitrogen Supply

At $T_2$, in shoot, AM222 distinctly clustered from the other genotypes. It included higher granule-bound starch synthase (*WAXY*; SMEL_000g036450.1) transcript levels together with a significant higher D-glucose accumulation; by contrast, a downregulation of (S)-2-hydroxy-acid oxidase (*HAO*; SMEL_007g292380.1) histidyl-tRNA synthetase (*HARS*;

SMEL_003g195740.1), which correlated with a high accumulation in the primary metabolites D-fructose, shikimic, and quinic acids was observed. In addition, AM222 showed a high polyphenol oxidase (*PPO*; SMEL_008g312510.1) and phenyl alanine ammonia-lyase (*PAL*; SMEL_005g230690.1) expression in the phenylalanine metabolism as well as two and three genes in the glyoxylate and dicarboxylate and starch and sucrose metabolisms, respectively. In this last pathway, two sucrose synthase (*SUS*; SMEL_007g277310.1 and SMEL_007g277290.1) isoforms and the fructokinase (*scrK*; SMEL_006g265210.1) appeared upregulated in AM222 and 67-3 (Supplementary Figure S5A).

AM22 and 305E40 were mainly distinguishable from the N-use-efficient genotypes for a large cluster of correlation, in which a higher catalase (*CAT*; SMEL_000g061370.1), (S)-2-hydroxy-acid oxidase (*HAO*; SMEL_007g292380.1), glycine dehydrogenase (*GLDC*; SMEL_008g307820.1), and isocitrate lyase (*aceA*; SMEL_007g288630.1) transcript abundances belonging to the glyoxylate and dicarboxylate metabolism were observed, together with a higher accumulation in the fumaric and dehydroascorbic acids as well as in L-serine, L-alanine, and L-asparagine (Supplementary Figure S5A).

At $T_2$, in root, AM222 showed an upregulation of the aspartyl-tRNA synthetase (*DARS2*; SMEL_000g033540.1), glucose-1-phosphate adenylyl transferase (*glgC*; SMEL_007g292070.1) and glyoxylate/succinic semialdehyde reductase (*GLYR*; SMEL_000g004100.1), accompanied by a higher accumulation in sucrose and amino acids L-alanine and glycine. It also showed a higher expression in the phenylalanine ammonia-lyase (*PAL*; SMEL_005g230690.1) sucrose synthase (*SUS*; SMEL_007g277290.1), two glycine hydroxy methyltransferase isoforms (*glyA*; SMEL_005g228290.1 and SMEL_005g241460.1), and a glycine cleavage system H protein (*gcvH*; SMEL_000g091530.1) belonging to glycine, serine, and threonine metabolism, accompanied by a higher accumulation in the amino acid L-asparagine compared to the other genotypes (Supplementary Figure S5B).

Otherwise, AM22 showed a distinguishable cluster of correlation including a strong downregulation of the starch synthase (*glgA*; SMEL_000g085440.1) and aspartyl-tRNA synthetase (*DARS2*; SMEL_000g033540.1) together with a very low sucrose accumulation. It also displayed a higher threonine synthase (*thrC*; SMEL_003g197730.1) and amidophosphoribosyltransferase (*purF*; SMEL_001g116660.1) transcript abundance compared to the other genotypes (Supplementary Figure S5B).

### 2.9. Implementing a Simplified Modeling Scheme

Overall, genes and metabolites that allowed for discrimination of the N-use-efficient vs. inefficient genotypes mainly belonged to the glycine, serine, and threonine (Supplementary Figure S6); glyoxylate and dicarboxylate (Supplementary Figure S7); and the starch and sucrose metabolism pathways (Supplementary Figure S8). In particular, at $T_0$, N-use-efficient genotypes showed a higher *asd* (i.e., aspartate-semialdehyde dehydrogenase) transcript abundance in the glycine, serine, and threonine metabolism. This gene forms a branch with the metabolic pathway making lysine, methionine, leucine, and isoleucine from aspartate. The same genotypes also showed a glycine hydroxymethyltransferase (*glyA*; SMEL_005g228290.1) downregulation, useful for the concurrent conversions of L-serine to glycine and tetrahydrofolate (THF) to 5,10-methylenetetrahydrofolate (Supplementary Figure S6A). Conversely, at $T_1$ and $T_2$, *asd* and *glyA* showed an inverted expression trend in the efficient genotypes, resulting in a higher *glyA* and lower *asd* expression compared to the inefficient ones (Supplementary Figure S6B,C). As a consequence, a higher level of glycine as well as of the glycine-cleavage-system H protein (*gcvH*) and dihydrolipoamide dehydrogenase (*DLD*) expression that regulates the glycine concentration and cell energy metabolism, respectively, was observed. By contrast, a higher accumulation of serine and glyceric acid, together with the upregulation of *AGXT* (alanine-glyoxylate transaminase) and *GLCD* (glycine dehydrogenase) was detected in the N-use-inefficient genotypes (Supplementary Figure S6B,C).

In the glyoxylate and dicarboxylate metabolism, the N-use-efficient genotypes showed *aceA* (isocitrate lyase) upregulation in the glyoxylate cycle, as well as a higher accumulation

in *HAO* [(S)-2-hydroxy-acid oxidase] and *CAT* (catalase) transcripts involved in the photorespiration cycle, and a low accumulation of *glyA* compared to the inefficient ones at N starvation ($T_0$) (Supplementary Figure S7A). At $T_1$, the N-use-efficient genotypes showed a significant downregulation of some transcripts involved in the glyoxylate cycle, such as *CS* (citrate synthase), *ACO* (aconitate hydratase), and *aceA* (isocitrate lyase), as well as *AGXT* (alanine-glyoxylate transaminase) and *HPR2_3* (glyoxylate/hydroxypyruvate reductase) involved in the photorespiration cycle; by contrast, *CAT* (catalase) and *glyA* (glycine hydroxymethyltransferase) resulted in upregulation (Supplementary Figure S7B).

Otherwise, at $T_2$, the N-use-efficient genotypes exhibited a significant upregulation of *ACO* and *glyA* transcripts and a higher accumulation in glycine; by contrast, a downregulation of *MDH* (malate dehydrogenase) and *aceA* involved in the glyoxylate cycle, as well as *HAO*, *CAT*, *AGXT*, *rbcL* (ribulose-bisphosphate carboxylase large chain), and *GLDC* (glycine dehydrogenase) in the photorespiration cycle, together with a consistent reduction of glyceric acid, were observed (Supplementary Figure S7C). In the starch and sucrose metabolism, at $T_0$, the N-use-efficient compared to the inefficient genotypes showed a significantly higher expression of *SUS* (sucrose synthase) and *E3.2.1.4* (endoglucanase), while the *INV* (invertase), *GN4* (glucan endo-1,3-beta-glucosidase 4) and *TPS* (trehalose 6-phosphate synthase/phosphatase) resulted in downregulation (Supplementary Figure S8A). At $T_1$, the N-use-efficient genotypes exhibited a higher transcript accumulation in the *WAXY* and *endoglucanase*, which are upstream amylose and cellobiose biosynthesis, together with the downregulation of *SUS*, *scrK* (fructokinase), and *TPS* genes, which resulted in a lower accumulation of sucrose (Supplementary Figure S8B). Conversely, at $T_2$, in the N-use-efficient genotypes we observed an upregulation of *SUS* and *scrK*, as well as a higher accumulation of D-glucose and D-fructose; meanwhile, *WAXY*, *endoglucanase*, and *glgC* (glucose-1-phosphate adenyltransferase) appeared strongly downregulated (Supplementary Figure S8C).

## 3. Discussion

In this study, combined metabolomics and transcriptomics analysis in two pairs of NUE-contrasting eggplant genotypes, AM222, 67-3 (high NUE); and 305E40, AM22 (low NUE) was performed, in root and shoot, under short- and long-term N-limiting conditions. Plant responses to low N resupply in NUE-contrasting genotypes are of particular interest to dissect the key molecular mechanisms underlying this complex trait, to identify the critical steps controlling NUE, and to provide new insights for breeding programs to improve NUE. Here, the base for deciphering metabolites and gene-correlation networks to facilitate NUE improvement in eggplant was provided, as previously reported in other crops [21,22].

### 3.1. Variance and Pathway Analysis

At all the sampling times, root showed similar primary metabolite profiles regardless of genotype, while variations were mostly detected in the secondary metabolites. By contrast, in shoot, variations in primary metabolites were revealed across sampling times (except for the genotype AM22) and between genotypes when compared at the same sampling time. To explore these differences, all the possible pairwise comparisons were performed between the most N-use-inefficient genotype, AM22, and the other genotypes, allowing us to highlight the affected pathways in this tissue.

Under N starvation ($T_0$), the content of most amino acids was reduced in the N-use-efficient genotypes, mainly L-glutamine. Low levels of N-containing metabolites, such as glutamate and glutamine, and C-containing compounds were already observed under N starvation together with an elevated level of organic acids, suggesting their utilization to build macromolecules [20]. At $T_1$, L-aspartate and L-asparagine, belonging to the alanine, aspartate, and glutamate pathway, resulted in an increase in N-use-efficient genotypes. In detail, L-asparagine, the amino acid with the highest N:C ratio, plays an important role in N transport and storage through the vascular system, or alternatively accumulates

in response to stress, contributing to osmotic-pressure maintenance [23]. Finally, after a long-term N-limiting condition (T$_2$), AM222 showed a higher accumulation in D-glucose and sucrose (starch and sucrose metabolism), while 67-3 evidenced a reduction in all the metabolites in the alanine, aspartate, and glutamate metabolism, but a slight L-glutamine accumulation. Sugars frequently play an important role as osmoprotectors, as membrane stabilizers, in stress buffering [24], as well as in the regulation of growth, photosynthesis, carbon partitioning, carbohydrate and lipid metabolism, protein synthesis, and gene expression [25]. Interestingly, the most N-use-efficient genotype AM222 compared to the other genotypes showed higher accumulation of phenylalanine and citric acid that were reported to confer tolerance to abiotic stress, improving growth and yield in many crop species [26]. By contrast, an increase in proline and alanine in the N-use-inefficient genotype AM22 could indicate prolonged stress due to the unbalanced N supply [27]. Indeed, it is well-known that proline accumulates in plants subjected to environmental stress [28], maintaining osmotic balance and protecting cells against ROS under salt stress [29]. The biological significance of the alanine accumulation in plants is still controversial; indeed, its accumulation may be a N-storage mechanism, before restoring to an N-normal condition [30]. Thus, it is more difficult to explain the alanine increase in the N-use-inefficient genotypes. In the last decade, many efforts have been carried out to improve NUE through genetic engineering by overexpressing N-assimilation genes, among which includes the *alanine aminotransferase* (*AlaAT*) [31]. However, inconsistent results were obtained from transgenic plants evaluated under field conditions, suggesting that the overexpression of N-assimilation genes may cause metabolic imbalances [32,33].

### 3.2. Metabolite and Transcript Correlation Analysis

Metabolomics and transcriptomic data were analyzed by Pearson correlation analysis to identify genes and metabolites that concurrently distinguished N-use-efficient and inefficient eggplant genotypes. In accordance to Cavill et al. [34], our analyses integrated a subset of 121 genes and 39 metabolites (primary and secondary), resulting into 70 variables (47 transcripts and 23 metabolites). The correlation heatmaps between genes and metabolites showed different clusters in which AM222 and AM22 (the extreme NUE-contrasting genotypes) were always well-distinguished in both shoot and root.

Our findings suggest that differences between the two pairs of NUE-contrasting genotypes in secondary-metabolite biosynthesis; glyoxylate and dicarboxylate; glycine, serine, and threonine; and starch and sucrose metabolism pathways could be crucial for N-use efficiency in eggplant, in both the short and long term (T$_1$ and T$_2$). In agreement, DEGs and metabolic changes in amino acid, carbon, and nitrogen metabolism pathways were observed between two NUE-contrasting cotton genotypes in response to N starvation and resupply treatments [35]. These results showed an enrichment in the starch and sucrose metabolism, glycolysis/gluconeogenesis, and pentose phosphate pathways in N-use-efficient cotton genotypes, underlying that plant-energy budget as well as carbon and nitrogen metabolism and their balance are involved in the different NUE performances [35,36]. By contrast, in our experiments the N-use-inefficient genotypes showed a significant higher fumaric acid accumulation, previously observed in a starchless *pgm1* mutant [37]. This implied that fumaric acid and starch should serve as alternative carbon sinks for photosynthate, resulting in an effective higher N assimilation and *Arabidopsis* growth only when high N is available [38].

Interestingly, a significant PPOs upregulation at long-term low-N stress in AM222, the high-NUE genotype, was observed. Phenol-oxidizing enzymes are responsible of browning enzymatic reaction in post-harvest fruits and vegetables; although the PPOs' native physiological functions in intact and undamaged plant cells are not still understood to date [39]. Recently, PPOs were reported to play different roles in response to plant stress in several species and may have an indirect role in photosynthesis [40]. By contrast, two different polyphenol oxidases (PPOs), an unsaturated malonyl solamargine and an

unknown steroidal saponin, resulted in upregulation/accumulation in the N-use-inefficient eggplant genotypes, at both N-starvation ($T_0$) and short-term low-N stress ($T_1$).

### 3.3. Glycine, Serine, and Threonine Metabolism

Glycine is the main player of this pathway, which also includes the serine and betaine biosynthesis, which have been reported to be involved in plant responses to abiotic stress [41–43]. At $T_0$, we observed in the N-use-efficient genotypes a very low level of *glyA* transcript encoding the enzyme, converting L-serine to glycine and tetrahydrofolate (THF). Furthermore, a higher aspartate-semialdehyde dehydrogenase (ASD) gene expression in trehalose biosynthesis sustains the formation of lysine and other amino acids from aspartate. Interestingly, under short- and long-term low-N stress (at $T_1$ and $T_2$), *glyA* (also named *shmt1*) inverted the expression trend, resulting in an increase in both AM222 and 67-3 compared to the N-use-inefficient genotypes. A high *shmt1* transcript level was reported, correlating with a reduced sensitivity to abiotic stress in *Arabidopsis* [42]. The higher *glyA* expression in the N-use-efficient genotypes resulted in very high glycine accumulation, mainly at $T_2$, which could sustain the betaine formation, two primary metabolites that were reported to accumulate under abiotic stress in rice and several other plants [41,43]. More interestingly, the regulation of the glycine-concentration and the cell-energy metabolism appeared to be further guaranteed by a higher glycine-cleavage-system H protein (*gcvH*) and dihydrolipoamide dehydrogenase (*DLD*) expression in these genotypes.

By contrast, a higher accumulation of serine and glyceric acid (instead of glycine) in the N-use-inefficient genotypes appeared sustained by the *glyA* (=*shmt1*) downregulation together with a significant upregulation of *AGXT* (alanine-glyoxylate transaminase).

### 3.4. Glyoxylate and Dicarboxylate Metabolism

In plants, glyoxysomes frequently store lipids, and through the glyoxylate cycle, they are involved in the conversion of acetyl-CoA to succinate for the synthesis of carbohydrates. Under N starvation ($T_0$), the N-use-efficient compared to inefficient genotypes exhibited a higher *aceA* transcript abundance. *AceA* encodes for isocitrate lyase, a key enzyme in the glyoxylate cycle that could play a pivotal role in energy metabolism for facing up stress as described by Yuenyong et al. [44]. The *HAO* (S)-2-hydroxy-acid oxidase) and *CAT* (catalase) upregulation in the same genotypes could also act on the glycolate–glyoxylate conversion for preventing the accumulation of glycolate and hydrogen peroxide at toxic levels as reported in maize [45].

Afterwards, at short low-N stress ($T_1$), in the N-use-efficient genotypes an upregulation of *glyA* (*shmt1*), involved in the photorespiration cycle, was observed. The encoded enzyme catalyzes the interconversion of glycine (glyoxylate-derived) to serine and tetrahydrofolate (THF) acting as a carbon carrier. These compounds, accompanied to a higher *CAT* expression, could mitigate oxidative stress, driving an abiotic stress tolerance as already observed in *Arabidopsis* [46]. By contrast, *CS*, *ACO*, and *aceA* were downregulated in the efficient genotypes, and in particular, the inhibition of ACO activity was useful for plants to cope with oxidative stress, also correlating with cell death [47].

At the long-term N-stress ($T_2$), *glyA* resulted in upregulation, together with a higher glycine accumulation in the N-use-efficient genotypes. Interestingly, this amino acid and its derivative, glycinbetaine, were more accumulated under abiotic stress in rice and other plant species [41,43]. By contrast, *aceA* and the malate dehydrogenase (MDH) genes downregulation resulted in an efficient redox activity of the mitochondrial matrix as reported in *Arabidopsis* [48]. Furthermore, among the major players in the photorespiration pathway, a central role is attributed to *HAO*, *CAT*, *rbcL*, *GLDC*, *AGXT*, and glyceric acid, which were highly accumulated in the N-use-inefficient genotypes under low N exposure, suggesting that they consumed more energy in photorespiration compared to the N-use-efficient ones.

### 3.5. Starch and Sucrose Metabolism

Sucrose is a raw material for many metabolic pathways, providing energy and carbon skeletons to macromolecules. Otherwise, starch plays a dual role in carbon allocation, acting as both a source, releasing carbon reserves in leaves for growth and development; and a sink, either as a dedicated starch store (seeds) or a temporary reserve of carbon contributing to sink strength in reproductive organs (flowers and fruits) [49].

In this pathway, different behaviors between the two pairs of NUE-contrasting genotypes were observed. Under N starvation ($T_0$), the genes upstream of the fructose, glucose, and trehalose synthesis (*INV*, *GN4*, and *TPS*, respectively) were downregulated in the N-use-efficient compared to the inefficient genotypes, while sucrose synthase (*SUS*) and *endoglucanase* resulted in higher transcripts. Thus, the N-use-efficient genotypes utilized *SUS* to synthesize sucrose, while the inefficient ones hydrolyzed sucrose by invertase (encoded by *INV*) to produce glucose and fructose.

At $T_1$, N-use-efficient genotypes exhibited a *WAXY* and *endoglucanase* (*E3.2.1.4*) up-regulation, both playing a central role in the starch and amylose biosynthesis [50]. Endoglucanase contributes to the cellulose catabolic process during tissue development and cellulose degradation, making available the monosaccharides for consumption in chemical reactions [51]. By contrast, N-use-inefficient genotypes showed a higher sucrose accumulation, as well as *scrK*, *SUS*, and *TPS* transcript abundances. In detail, a high *TPS*-transcript abundance suggested a plant response to abiotic stress, causing a reduction in plant growth [52]. By contrast, the long-term low N exposure ($T_2$) determined a *WAXY* and *endoglucanase* downregulation in the N-use efficient genotypes that in turns showed a *SUS* and *fructokinase* up-regulation as well as a higher fructose and glucose accumulation. It appears that the N-use-inefficient genotypes turn to cellulose degradation and starch biosynthesis (higher *WAXY*, *glgC*, and *endoglucanase* transcript accumulation was observed).

## 4. Materials and Methods

### 4.1. Plant Materials, Experimental Design, Tissue Sampling, and Sample Preparation

Two pairs of NUE-contrasting eggplants, named AM22, AM222, 67-3, and 305E40 were selected through hydroponic and greenhouse experiments [14]. In detail, AM222 and 67-3 were the N-use-efficient genotypes, while 305E40 and AM22 were the inefficient ones. Seeds, surface-sterilized with NaClO 5% (*v*/*v*) for 15 min and rinsed with deionized water, were germinated in Petri dishes (Ø 90 mm) on filter paper enriched with 0.1 mM $CaSO_4$. After 10 days, seedlings with fully expanded cotyledons were selected and transferred to hydroponic tanks (4 L, ten seedlings per tank) containing 2.5 mM $K_2SO_4$, 2 mM $MgSO_4$, 1 mM $KH_2PO_4$, 46 μM $H_3BO_3$, 9 μM $MnCl_2$, 0.76 μM $ZnSO_4$, 0.32 μM $CuSO_4$, 0.11 μM $Na_2MoO_4$, 20 μM Fe-EDTA, and 4.75 mM $CaSO_4$. The growing units were then transferred to a growth chamber at 24 °C, 65% relative humidity, and 14 h photoperiod with photon flux density of 350 μmol $m^{-2}$ $s^{-1}$ at plant height generated by high-pressure sodium discharge lamps. After two additional days, 0.5 mM $NO_3^-$ (as $CaNO_3$) was added to the solution, and seedlings were grown for further 16 d. The nutrient solution was renewed every three days, and the pH was adjusted to 5.8 with 1 N KOH. Each genotype and tissue (root and shoot) were collected at $T_0$ (before N supply), $T_1$ and $T_2$ (1 and 16 days after $NO_3^-$ resupply). Three biological replicates, consisting of eight bulked plants per replication for each tissue (root and shoot) after four hours of exposure to light were collected. The stored tissues were then powdered using an ice-cold mortar and pestle with liquid nitrogen for extraction of metabolites.

### 4.2. Metabolite Extraction and Annotation

The polar-metabolite extraction and derivatization for untargeted analysis by Gas Chromatography–Mass Spectrometry (GC-MS) using the method from Korenblum et al. [53] were carried out. The annotation was made by matching retention index and mass-spectrum data to the commercial Mass Spectral Library, NIST (www.nist.gov, 8 January 2022). The extraction of semipolar compounds for LCMS analysis by an ultra-high-performance liquid

chromatography-quadrupole time-of-flight mass spectrometry (UPLC-qTOF-MS) (HDMS Synapt; Waters) was performed according to Itkin et al. [54] and the analyses were made according to Korenblum et al. [53]. Metabolites, comparing the retention times and the mass fragments to those of standard compounds injected at the same LCMS conditions, were identified. Compounds were putatively identified by comparing their retention times, elemental composition, and fragmentation pattern (MSE or ms/ms) with the home-made library, or as described in the literature when corresponding standards were not available.

### 4.3. RNAseq Analysis Data Validation by qRT-PCR

RNAseq analysis was previously carried out, and the most interesting identified DEGs validated by qRT-PCR [15]. Briefly, total RNA was isolated and purified using the Mini RNeasy Plant kit (QIAGEN, Milano, Italy), and 500 ng of total RNA per sample was used to construct cDNA libraries following the Transeq library procedures reported in Tzfadia et al. [55]. Libraries were sequenced on six lanes of HiSeq 2500 System (Illumina, San Diego, CA, USA), using the SR60 protocol. The Transeq output was ~3 million reads per sample. Resulting reads shorter than 30 bp were discarded and mapped to eggplant reference genome SMEL_V3.2016_11_01 from the Italian Consortium [56] using STAR vers. 2.4.2a (with EndToEnd option and outFilterMismatchNoverLmax was set to 0.04) [57]. RNAseq data were validated by using qRT-PCR analysis performed on a StepOnePlus Real-Time PCR System (Applied Biosystems, Life Technologies Corporation, Foster City, CA, USA), following the procedures reported by Mauceri et al. [14,15].

### 4.4. Statistical Analysis for Metabolite Profiling

Metabolomic analyses were performed in triplicate using a completely randomized experimental design, as reported in Section 4.1, and analyzed through the open-source software MetaboAnalyst 4.0 (www.metaboanalyst.ca, 9 January 2022) web [58]. Missing values were replaced by a small positive value (half of the minimum positive number detected in the data) and features with >50% missing values were removed. Then, raw data were normalized by a reference metabolite (ribitol), log10-transformed, and Pareto scaled [59]. The datasets were reduced by performing principal component analysis (PCA) and the partial least-squares discriminant analysis (PLS-DA). The model was validated and classified based on $Q^2 = 0.719$ and $R^2 = 0.906$. Twenty permutations with the *p*-value test < 0.05 were carried out. The score plots visualized the contrast between samples and the loading plots to explain the cluster separation with the variable importance of projection (VIP) score as cutoff $\geq 1$. Data analyses were performed through the ANOVA univariate analysis using the least-significant difference (Fisher's LSD) ($p \leq 0.05$) as post hoc tests adjusted *p*-value (FDR) cutoff ($\leq 0.05$). To create a graphical heatmap with complete pairwise, a hierarchical clustering algorithm was adopted, and a Pearson correlation as distance measure was calculated.

### 4.5. KEGG Orthology (KO) Annotation and Transcriptomics and Metabolomics Integrated Correlation Network Analysis

RNAseq transcripts were functionally annotated using the Kyoto Encyclopaedia of Genes and Genomes (KEGG) database, and the R statistical package 'Hmisc'v4.4-2 with Functions "rcorr" to estimate the Pearson Correlation Coefficient was used. Genes and metabolite-network analysis was carried out using MetScape v3.1 and Cytoscape v3.8.1, respectively. Correlation thresholds were defined using Pearson correlation coefficient (PCC) $\geq 0.70$ and $\leq -0.70$ with *p*-value < 0.05. To obtain ENTREZ ID from symbol *Arabidopsis* ortholog of eggplant gene, a R-statistical package 'org.At.tair.db' v3.13 was employed. The integrated metabolic-pathway analysis among metabolomics and gene expressions was conducted by the Joint Pathway Analysis module (MetaboAnalyst 4.0). A graphical heatmap by the function "pheatmap" (package pheatmap) with the pairwise complete and Pearson method was created [60]. Pair comparisons were performed using volcano plot

with FDR p-adjusted < 0.05) with LOG2 (FC) $\geq \pm 1$ through statistical analysis module of the open-source software MetaboAnalyst 4.0 (www.metaboanalyst.ca, 9 Juanary 2022).

## 5. Conclusions

Multivariate analyses of primary and secondary metabolites contributed to a better understanding of NUE-contrasting eggplant plant responses. These approaches indicated that primary and secondary metabolites were affected by N stress in shoot and root, respectively. The analysis of these metabolites and their roles in each pathway showed that short- and long-term low N availability impacted the number and accumulation of specific classes of primary metabolites such as amino acids, sugars, and organic acids in the N-use-efficient genotypes.

Our study displayed differences among genotypes mainly in the shoot than in root; in detail, six different pathways appeared the most affected. Moreover, an integrated analysis between differential accumulated metabolites and expressed transcripts highlighted a central role of the glycine, serine, and threonine; glyoxylate and dicarboxylate; as well as starch and sucrose metabolisms. In the first two pathways, glycine and the related enzyme *glyA* seem to play a significant role in plant N-stress responses in the N-use-efficient genotypes. After two days of N starvation, an alternative higher accumulation of serine and glyceric acid in the N-use-inefficient genotypes was observed. A correlation between *SUS* and *fructokinase* transcript abundances and the D-glucose and D-fructose accumulation appeared useful to distinguish N-use-efficient and inefficient genotypes in starch and sucrose metabolism. Interestingly, at long-term low N exposure, a *WAXY* and *endoglucanase* downregulation in the N-use-efficient genotypes was evident, together with a *SUS* and *fructokinase* upregulation. By contrast, the N-use-inefficient genotypes turn towards cellulose degradation and starch synthesis (higher *WAXY*, *glgC*, and *endoglucanase* transcript accumulation was observed).

The responses observed in the N-use-efficient compared to the most inefficient genotype AM22 could represent a starting point for a deeper understanding of the mechanisms of eggplant adaptation to low N. Therefore, key transcripts and metabolites and their pathways unveiled in this study could be used as potential candidate targets for eggplant-NUE improvement.

**Supplementary Materials:** The following supporting information can be downloaded at: https://www.mdpi.com/article/10.3390/plants11050700/s1. Figure S1—Interactive visualization system and detailed results from the pathway analysis in shoot are presented graphically for AM222, 67-3, and 305E40 vs. AM22: (A) and (B) to T0; (C–E) to T1; (F–H) to T2. Paths with FDR < 0.05 and with a higher Impact value were highlighted. A *p*-value of less than 0.05, 0.01, and 0.001 was designated with one (*), two (**), or three (***) asterisks, respectively. Figure S2—Correlation network between regulatory genes and related metabolites. The networks between metabolites and transcripts was performed with MetScape, bioinformatics framework for the visualization and interpretation of metabolomic data using Cytoscape software (version 3.8.1). Positive correlation is marked with red (A) and inverse correlation is marked with blue (B). Pathway-enrichment analysis and pathway impact for both metabolites and metabolic genes (C). Figure S3—Heatmap of correlations in eggplant accession between metabolites and transcripts by the Pearson's correlation coefficient (*p* < 0.05) at T0. Correlations between eggplant metabolites and transcripts are based on 70 variables in shoot (A) and root (B). Figure S4—Heatmap of correlations in eggplant accession between metabolites and transcripts by the Pearson's correlation coefficient (*p* < 0.05) at T1. Correlations between eggplant metabolites and transcripts are based on 70 variables in shoot (A) and root (B); Figure S5. Heatmap of correlations in eggplant accession between metabolites and transcripts by the Pearson's correlation coefficient (*p* < 0.05) at T2. Correlations between eggplant metabolites and transcripts are based on 70 variables in shoot (A) and root (B). Figure S6—Exemplary scheme of glycine, serine, and threonine metabolism between efficient vs. inefficient genotypes in shoots: A, T0; B, T1; and C. T2. In gray, the metabolites and metabolic genes identified and not statistically different; in green, the upregulated; and in yellow, the downregulated. Figure S7—Exemplary scheme of glyoxylate and dicarboxylate metabolism between efficient vs. inefficient genotypes in shoots: A, T0; B, T1;

C, T2. In gray, the metabolites and metabolic genes identified and not statistically different; in green, the upregulated; and in yellow, the downregulated. In red, the pathway modules relating to the glyoxylate cycle and photorespiration. Figure S8—Exemplary scheme of starch and sucrose metabolism between efficient vs. inefficient genotypes in shoots: A, T0; B, T1; C, T2. In gray, the metabolites and metabolic genes identified and not statistically different; in green, the upregulated; and in yellow, the downregulated. In red, the pathway modules relating to the glycogen biosynthesis and trehalose biosynthesis. Table S1—A: Putative metabolites identified from eggplant roots and shoots by GC–MS; B: Putative metabolites identified from eggplant roots and shoots by UPLC-QTOF-MS analysis. Table S2—(A) Loading plot root and (B) Loading plot shoot. Marked in yellow, variable with cutoff $+/-0.14$. Table S3—Partial least-squares discriminant analysis (PLS-DA) based on variable importance in projection (VIP) measure for each single metabolite. They are taken into consideration starting from a VIP score of 1 in shoot. Table S4—(A) root and (B) shoot metabolites. One-way ANOVA and post hoc tests adjusted *p*-value (FDR) cutoff: 0.05 Post hoc analysis: Fisher's LSD. Differences between genotypes at the same time marked in yellow. Marked in green, the differences for the same genotype at different times. No marked differences between genotypes at different times. Table S5—Results from pathway analysis are presented in a detailed table, from letter "A–F" the pairwise comparison about genotypes. Table S6—KEGG reference pathways, a subset of 121 genes were obtained overall. Table S7—Pearson's correlation coefficient (A) and *p*-value (B) of accession-specific metabolites and metabolic genes. Table S8—Pair comparisons: variables with significantly altered levels are indicated in detailed data table (FDR p-adjusted < 0.05). Variables with LOG2 (FC) $\geq \pm 1$ are marked in yellow. (A) T0, (B) T1, and (C) T2.

# References

1. Hirel, B.; Le Gouis, J.; Ney, B.; Gallais, A. The challenge of improving nitrogen use efficiency in crop plants: Towards a more central role for genetic variability and quantitative genetics within integrated approaches. *J. Exp. Bot.* **2007**, *58*, 2369–2387. [CrossRef] [PubMed]
2. Vitousek, P.M.; Mooney, H.A.; Lubchenco, J.; Melillo, J.M. Human Domination of Earth's Ecosystems. *Science* **1997**, *277*, 494. [CrossRef]
3. McArthur, J.W.; McCord, G.C. Fertilizing growth: Agricultural inputs and their effects in economic development. *J. Dev. Econ.* **2017**, *127*, 133–152. [CrossRef] [PubMed]
4. Rodriguez-Galiano, V.F.; Luque-Espinar, J.A.; Chica-Olmo, M.; Mendes, M.P. Feature selection approaches for predictive modelling of groundwater nitrate pollution: An evaluation of filters, embedded and wrapper methods. *Sci. Total Environ.* **2018**, *624*, 661–672. [CrossRef] [PubMed]
5. Correia, C.M.; Brito, C.; Sampaio, A.; Dias, A.A.; Bacelar, E.; Gonçalves, B.; Ferreira, H.; Moutinho-Pereira, J.; Rodrigues, M.A. Leguminous Cover Crops Improve the Profitability and the Sustainability of Rainfed Olive (*Olea europaea* L.). Orchards: From Soil Biology to Physiology of Yield Determination. *Proc. Environ. Sci.* **2015**, *29*, 282–283. [CrossRef]
6. Moll, R.H.; Kamprath, E.J.; Jackson, W.A. Analysis and Interpretation of Factors Which Contribute to Efficiency of Nitrogen Utilization. *Agron. J.* **1982**, *74*, 562–564. [CrossRef]
7. Good, A.G.; Shrawat, A.K.; Muench, D.G. Can less yield more? Is reducing nutrient input into the environment compatible with maintaining crop production? *Trends Plant Sci.* **2004**, *9*, 597–605. [CrossRef]
8. Hawkesford, M.J.; Griffiths, S. Exploiting genetic variation in nitrogen use efficiency for cereal crop improvement. *Curr. Opin. Plant Biol.* **2019**, *49*, 35–42. [CrossRef]

9. Allwood, J.W.; Xu, Y.; Martinez-Martin, P.; Palau, R.; Cowan, A.; Goodacre, R.; Marshall, A.; Stewart, D.; Howarth, C. Rapid UHPLC-MS metabolite profiling and phenotypic assays reveal genotypic impacts of nitrogen supplementation in oats. *Metabolomics* **2019**, *15*, 42. [CrossRef]

10. Mibei, E.A.-O.; Owino, W.O.; Ambuko, J.; Giovannoni, J.J.; Onyango, A.N. Metabolomic analyses to evaluate the effect of drought stress on selected African Eggplant accessions. *J. Sci. Food Agric.* **2018**, *98*, 205–216. [CrossRef]

11. Yang, R.; Yang, J.; Yu, J.; Wang, S.; Yang, C.; Xu, F. Effects of different nitrogen application rates on the quality and metabolomics of cigar tobacco. *Agron. J.* **2022**, 1–13. [CrossRef]

12. Li, H.; Hu, B.; Chu, C. Nitrogen use efficiency in crops: Lessons from *Arabidopsis* and rice. *J. Exp. Bot.* **2017**, *68*, 2477–2488. [CrossRef] [PubMed]

13. Hazra, P.; Rout, A.; Roy, U.; Nath, S.; Roy, T.; Dutta, R.; Acharya, S.; Mondal, A. Characterization of brinjal (*Solanum melongena* L.) germplasm. *Veg. Sci.* **2003**, *30*, 145–149.

14. Mauceri, A.; Bassolino, L.; Lupini, A.; Badeck, F.; Rizza, F.; Schiavi, M.; Toppino, L.; Abenavoli, M.R.; Rotino, G.L.; Sunseri, F. Genetic variation in eggplant for Nitrogen Use Efficiency under contrasting $NO_3^-$ supply. *J. Int. Plant Biol.* **2020**, *62*, 487–508. [CrossRef] [PubMed]

15. Mauceri, A.; Abenavoli, M.R.; Toppino, L.; Panda, S.; Mercati, F.; Aci, M.M.; Aharoni, A.; Sunseri, F.; Rotino, G.L.; Lupini, A. Transcriptomic insights on molecular regulation of *Solanum melongena* L. N-Use Efficiency. *J. Exp. Bot.* **2021**, *72*, 4237–4253. [CrossRef] [PubMed]

16. Hameed, A.; Ijaz, S.; Mohammad, I.S.; Muhammad, K.S.; Akhtar, N.; Khan, H.M.S. Aglycone solanidine and solasodine derivatives: A natural approach towards cancer. *Biomed. Pharmacother.* **2017**, *94*, 446–457. [CrossRef] [PubMed]

17. Lelario, F.; De Maria, S.; Rivelli, A.R.; Russo, D.; Milella, L.; Bufo, S.A.; Scrano, L. A Complete Survey of Glycoalkaloids Using LC-FTICR-MS and IRMPD in a Commercial Variety and a Local Landrace of Eggplant (*Solanum melongena* L.) and their Anticholinesterase and Antioxidant Activities. *Toxins* **2019**, *11*, 230. [CrossRef]

18. Krapp, A.; Berthomé, R.; Orsel, M.; Mercey-Boutet, S.; Yu, A.; Castaings, L.; Elftieh, S.; Major, H.; Renou, J.-P.; Daniel-Vedele, F. *Arabidopsis* roots and shoots show distinct temporal adaptation patterns toward nitrogen starvation. *Plant Physiol.* **2011**, *157*, 1255–1282. [CrossRef]

19. Ganie, A.H.; Pandey, R.; Kumar, M.N.; Chinnusamy, V.; Iqbal, M.; Ahmad, A. Metabolite Profiling and Network Analysis Reveal Coordinated Changes in Low-N Tolerant and Low-N Sensitive Maize Genotypes under Nitrogen Deficiency and Restoration Conditions. *Plants* **2020**, *11*, 1459. [CrossRef]

20. Lei, B.; Chang, W.; Zhao, H.; Zhang, K.; Yu, J.; Yu, S.; Cai, K.; Zhang, J.; Lu, K. Nitrogen application and differences in leaf number retained after topping affect the tobacco (*Nicotiana tabacum*) transcriptome and metabolome. *BMC Plant Biol.* **2022**, *22*, 38. [CrossRef]

21. Amiour, N.; Imbaud, S.; Clément, G.; Agier, N.; Zivy, M.; Valot, B.; Balliau, T.; Armengaud, P.; Quilleré, I.; Cañas, R.; et al. The use of metabolomics integrated with transcriptomic and proteomic studies for identifying key steps involved in the control of nitrogen metabolism in crops such as maize. *J. Exp. Bot.* **2012**, *63*, 5017–5033. [CrossRef] [PubMed]

22. Li, Z.; Hu, J.; Wu, Y.; Wang, J.; Song, H.; Chai, M.; Cong, L.; Miao, F.; Ma, L.; Tang, W.; et al. Integrative analysis of the metabolome and transcriptome reveal the phosphate deficiency response pathways of alfalfa. *Plant Physiol. Biochem.* **2022**, *170*, 49–63. [CrossRef] [PubMed]

23. Lea, P.J.; Sodek, L.; Parry, M.A.J.; Shewry, P.R.; Halford, N.G. Asparagine in plants. *Ann. Appl. Biol.* **2007**, *150*, 1–26. [CrossRef]

24. Braun, H.; Fontes, P.C.R.; Silva, T.P.D.; Finger, F.L.; Cecon, P.R.; Ferreira, A.P.S. Carbohydrates Concentration in leaves of potato plants affected by nitrogen fertilization rates. *Rev. Ceres* **2016**, *63*, 241–248. [CrossRef]

25. Renau-Morata, B.; Molina, R.-V.; Minguet, E.G.; Cebolla-Cornejo, J.; Carrillo, L.; Martí, R.; García-Carpintero, V.; Jiménez-Benavente, E.; Yang, L.; Cañizares, J.; et al. Integrative Transcriptomic and Metabolomic Analysis at Organ Scale Reveals Gene Modules Involved in the Responses to Suboptimal Nitrogen Supply in Tomato. *Agronomy* **2021**, *11*, 1320. [CrossRef]

26. Tahjib-Ul-Arif, M.; Zahan, M.I.; Karim, M.M.; Imran, S.; Hunter, C.T.; Islam, M.S.; Mia, M.A.; Hannan, M.A.; Rhaman, M.S.; Hossain, M.A.; et al. Citric Acid-Mediated Abiotic Stress Tolerance in Plants. *Int. J. Mol. Sci.* **2021**, *22*, 7235. [CrossRef]

27. Atanasova, E. Effect of nitrogen sources on the nitrogenous forms and accumulation of amino acid in head cabbage. *Plant Soil Environ.* **2008**, *54*, 66–71. [CrossRef]

28. Li, S.; Yan, L.; Riaz, M.; White, P.J.; Yi, C.; Wang, S.L.; Shi, L.; Xu, F.S.; Wang, C.; Cai, H.M.; et al. Integrated transcriptome and metabolome analysis reveals the physiological and molecular responses of allotetraploid rapeseed to ammonium toxicity. *Environ. Exp. Bot.* **2021**, *189*, 104550. [CrossRef]

29. Chourasia, K.N.; More, S.J.; Kumar, A.; Kumar, D.; Singh, B.; Bhardwaj, V.; Kumar, A.; Das, S.K.; Singh, R.K.; Zinta, G.; et al. Salinity responses and tolerance mechanisms in underground vegetable crops: An integrative review. *Planta* **2022**, *255*, 68. [CrossRef]

30. Khan, S.; Pinto, V.B.; do Amaral Júnior, A.T.; Gonçalves, G.M.B.; Corrêa, C.C.G.; Ferreira, F.R.A.; de Souza, G.A.R.; Campostrini, E.; Freitas, M.S.M.; Vieira, M.E.; et al. Revealing the differential protein profiles behind the nitrogen use efficiency in popcorn (*Zea mays* var. *everta*). *Sci. Rep.* **2022**, *12*, 1521. [CrossRef]

31. McAllister, C.H.; Beatty, P.H.; Good, A.G. Engineering nitrogen use efficient crop plants: The current status. *Plant Biotechnol. J.* **2012**, *10*, 1011–1025. [CrossRef] [PubMed]

32. Teng, W.; He, X.; Tong, Y.P. Transgenic approaches for improving use efficiency of nitrogen, phosphorus and potassium in crops. *J. Int. Agric.* **2017**, *16*, 2657–2673. [CrossRef]

33. Thomsen, H.C.; Eriksson, D.; Møller, I.S.; Schjoerring, J.K. Cytosolic glutamine synthetase: A target for improvement of crop nitrogen use efficiency? *Trends Plant Sci.* **2014**, *19*, 656–663. [CrossRef]

34. Cavill, R.; Jennen, D.; Kleinjans, J.; Briedé, J.J. Transcriptomic and metabolomic data integration. *Brief Bioinform.* **2016**, *17*, 891–901. [CrossRef]

35. Iqbal, A.; Dong, Q.; Wang, X.; Gui, H.; Zhang, H.; Zhang, X.; Song, M. Transcriptome Analysis Reveals Differences in Key Genes and Pathways Regulating Carbon and Nitrogen Metabolism in Cotton Genotypes under N Starvation and Resupply. *Int. J. Mol. Sci.* **2020**, *21*, 1500. [CrossRef] [PubMed]

36. Nunes-Nesi, A.; Fernie, A.R.; Stitt, M. Metabolic and signaling aspects underpinning the regulation of plant carbon nitrogen interactions. *Mol. Plant* **2010**, *3*, 973–996. [CrossRef]

37. Fürtauer, L.; Pschenitschnigg, A.; Scharkosi, H.; Weckwerth, W.; Nägele, T. Combined multivariate analysis and machine learning reveals a predictive module of metabolic stress response in *Arabidopsis thaliana*. *Mol. Omics* **2018**, *14*, 437–449. [CrossRef] [PubMed]

38. Pracharoenwattana, I.; Zhou, W.; Keech, O.; Francisco, P.B.; Udomchalothorn, T.; Tschoep, H.; Stitt, M.; Gibon, Y.; Smith, S.M. *Arabidopsis* has a cytosolic fumarase required for the massive allocation of photosynthate into fumaric acid and for rapid plant growth on high nitrogen. *Plant J.* **2010**, *62*, 785–795. [CrossRef] [PubMed]

39. Araji, S.; Grammer, T.A.; Gertzen, R.; Anderson, S.D.; Mikulic-Petkovsek, M.; Veberic, R.; Phu, M.L.; Solar, A.; Leslie, C.A.; Dandekar, A.M.; et al. Novel roles for the polyphenol oxidase enzyme in secondary metabolism and the regulation of cell death in walnut. *Plant Physiol.* **2014**, *164*, 1191–1203. [CrossRef]

40. Jukanti, A. Distribution, localization, and structure of plant polyphenol oxidases (PPOs). In *Polyphenol Oxidases (PPOs) in Plants*; Springer: Singapore, 2017; pp. 11–32.

41. Annunziata, M.G.; Ciarmiello, L.F.; Woodrow, P.; Dell'Aversana, E.; Carillo, P. Spatial and Temporal Profile of Glycine Betaine Accumulation in Plants Under Abiotic Stresses. *Front. Plant Sci.* **2019**, *10*, 230. [CrossRef]

42. Liu, Y.; Mauve, C.; Lamothe-Sibold, M.; Guérard, F.; Glab, N.; Hodges, M.; Jossier, M. Photorespiratory serine hydroxymethyl-transferase 1 activity impacts abiotic stress tolerance and stomatal closure. *Plant Cell Environ.* **2019**, *42*, 2567–2583. [CrossRef] [PubMed]

43. Xiaochuang, C.; Chu, Z.; Lianfeng, Z.; Junhua, Z.; Hussain, S.; Lianghuan, W.; Qianyu, J. Glycine increases cold tolerance in rice via the regulation of N uptake, physiological characteristics, and photosynthesis. *Plant Physiol. Biochem.* **2017**, *112*, 251–260. [CrossRef] [PubMed]

44. Yuenyong, W.; Sirikantaramas, S.; Qu, L.J.; Buaboocha, T. Isocitrate lyase plays important roles in plant salt tolerance. *BMC Plant Biol.* **2019**, *19*, 472. [CrossRef] [PubMed]

45. Schlüter, U.; Mascher, M.; Colmsee, C.; Scholz, U.; Bräutigam, A.; Fahnenstich, H.; Sonnewald, U. Maize source leaf adaptation to nitrogen deficiency affects not only nitrogen and carbon metabolism but also control of phosphate homeostasis. *Plant Physiol.* **2012**, *160*, 1384–1406. [CrossRef]

46. Moreno, J.I.; Martín, R.; Castresana, C. Arabidopsis SHMT1, a serine hydroxymethyl-transferase that functions in the photorespi-ratory pathway influences resistance to biotic and abiotic stress. *Plant J.* **2005**, *41*, 451–463. [CrossRef]

47. Moeder, W.; del Pozo, O.; Navarre, D.A.; Martin, G.B.; Klessig, D.F. Aconitase plays a role in regulating resistance to oxidative stress and cell death in *Arabidopsis* and *Nicotiana benthamiana*. *Plant Mol. Biol.* **2007**, *63*, 273–287. [CrossRef]

48. Lindén, P.; Keech, O.; Stenlund, H.; Gardeström, P.; Moritz, T. Reduced mitochondrial malate dehydrogenase activity has a strong effect on photorespiratory metabolism as revealed by 13C labelling. *J. Exp. Bot.* **2016**, *67*, 3123–3135. [CrossRef]

49. Yoshida, K.; Komae, K. A rice family 9 glycoside hydrolase isozyme with broad substrate specificity for hemicelluloses in type II cell walls. *Plant Cell Physiol.* **2006**, *47*, 1541–1554. [CrossRef]

50. Seung, D.; Soyk, S.; Coiro, M.; Maier, B.A.; Eicke, S.; Zeeman, S.C. Protein targeting to starch is required for localising granule-bound starch synthase to starch granules and for normal amylose synthesis in *Arabidopsis*. *PLoS Biol.* **2015**, *13*, e1002080. [CrossRef]

51. Zhang, Y.-H.P.; Lynd, L.R. Toward an aggregated understanding of enzymatic hydrolysis of cellulose: Non complexed cellulase system. *Biotechnol. Bioeng.* **2004**, *88*, 798–842. [CrossRef]

52. Sarkar, A.K.; Sadhukhan, S. Imperative role of trehalose metabolism and trehalose-6-phosphate signalling on salt stress responses in plants. *Physiol. Plant.* **2022**, e13647. [CrossRef]

53. Korenblum, E.; Dong, Y.; Szymanski, J.; Panda, S.; Jozwiak, A.; Massalha, H.; Meir, S.; Rogachev, I.; Aharoni, A. Rhizosphere microbiome mediates systemic root metabolite exudation by root-to-root signaling. *Proc. Natl. Acad. Sci. USA* **2020**, *117*, 3874–3883. [CrossRef] [PubMed]

54. Itkin, M.; Heinig, U.; Tzfadia, O.; Bhide, A.J.; Shinde, B.; Cardenas, P.D.; Bocobza, S.E.; Unger, T.; Malitsky, S.; Finkers, R.; et al. Biosynthesis of antinutritional alkaloids in solanaceous crops is mediated by clustered genes. *Science* **2013**, *341*, 175–179. [CrossRef] [PubMed]

55. Tzfadia, O.; Bocobza, S.; Defoort, J.; Almekias-Siegl, E.; Panda, S.; Levy, M.; Storme, V.; Rombauts, S.; Jaitin, D.A.; Keren-Shaul, H.; et al. The 'TranSeq' 3'-end sequencing method for high-throughput transcriptomics and gene space refinement in plant genomes. *Plant J.* **2018**, *96*, 223–232. [CrossRef] [PubMed]

56. Barchi, L.; Pietrella, M.; Venturini, L.; Minio, A.; Toppino, L.; Acquadro, A.; Andolfo, G.; Aprea, G.; Avanzato, C.; Bassolino, L.; et al. A chromosome-anchored eggplant genome sequence reveals key events in Solanaceae evolution. *Sci. Rep.* **2019**, *9*, 11769. [CrossRef]

57. Dobin, A.; Davis, C.A.; Schlesinger, F.; Drenkow, J.; Zaleski, C.; Jha, S.; Batut, P.; Chaisson, M.; Gingeras, T.R. STAR: Ultrafast universal RNA-seq aligner. *Bioinformatics* **2013**, *29*, 15–21. [CrossRef]

58. Xia, J.; Psychogios, N.; Young, N.; Wishart, D.S. MetaboAnalyst: A web server for metabolomic data analysis and interpretation. *Nucleic Acids Res.* **2009**, *37*, W652–W660. [CrossRef]

59. Van den Berg, R.A.; Hoefsloot, H.C.; Westerhuis, J.A.; Smilde, A.K.; van der Werf, M.J. Centering, scaling, and transformations: Improving the biological information content of metabolomics data. *BMC Genom.* **2006**, *7*, 142. [CrossRef]

60. Kolde, R. Pheatmap: Pretty Heatmaps. R Package Version 1.0.10. 2012. Available online: https://CRAN.R-project.org/package=pheatmap (accessed on 30 December 2021).